Grain-size dependence of magnetic microstructure and high-frequency susceptibility of nanocrystalline thin films: A micromagnetic simulation study

A.V. Izotov [a,b], B.A. Belyaev [a,b], P.N. Solovev [a,b,*], N.M. Boev [a,b]

[a] *Siberian Federal University, 79 Svobodny pr., Krasnoyarsk 660041, Russia*
[b] *Kirensky Institute of Physics, Federal Research Center KSC SB RAS, 50/38 Akademgorodok, Krasnoyarsk 660036, Russia*

A R T I C L E   I N F O

A B S T R A C T

The size of crystallites is one of the most important factors that determine the key characteristics of nanocrystalline thin magnetic films that make them very promising media for various applications. In this paper, using micromagnetic simulation, we study in detail the influence of the grain size on the magnetic microstructure of the films and its relation with high-frequency dynamics of magnetization. When the grain size exceeds some critical value D_{cr}, a sharp broadening and shift of the ferromagnetic resonance line are observed at certain frequencies of the alternating magnetic field. Using a two-magnon scattering model, it is shown that these effects are caused by the scattering of spin waves on the inhomogeneous stochastic magnetic structure—magnetization ripple. An expression for the determination of the critical size D_{cr} is obtained. The micromagnetic simulation results agree with the main conclusions of the static and dynamic theories of magnetization ripple and also confirmed by experimental data reported by other authors.

1. Introduction

Nanocrystalline soft magnetic materials have a set of unique properties rendering them advantageous over ferrites, mono- and polycrystalline materials traditionally used in microwave electronics. Usually, nanocrystalline alloys have higher values of the magnetization saturation and high-frequency magnetic susceptibility, which makes them particularly promising for microwave devices [1,2]. Among various nanocrystalline soft magnetic materials Fe-based alloys, such as FeCuNbSiB alloys [3,4], FeBNbCu alloys [5] and FeZrB(Cu) alloys [6] show attractive high-frequency characteristics. In addition to the high values of the magnetization saturation and initial susceptibility, they also demonstrate substantially lower eddy current losses compared to their crystalline analogs [7]. Currently, researchers also actively study soft magnetic FeCo-based alloys [8,9] that are promising for microwave applications.

Thin films and multilayers made of nanocrystalline magnetic materials are of special interest [10]. They have found applications as functional materials in devices compatible with planar technology. For instance, thin soft magnetic films are widely used as sensing elements in magnetic sensors of various types: in fluxgate [11] spin-dependent-tunneling [12] giant magnetoimpedance sensors [13] or sensors based on microstrip structures [14,15]. Furthermore, the use of nanocrystalline magnetic materials in the form of thin films and multilayers makes it possible to significantly increase their magnetic susceptibility and upper limit of the operating frequency range [16,17]. The relation between the magnetic susceptibility and frequency of ferromagnetic resonance (FMR), introduced by Acher and Adenot [18] clearly shows the superiority of thin-film magnetic materials over their bulk counterparts [17]. Another advantage in using thin films and multilayers lies in the fact that such structures allow for greater flexibility in choosing the composition of a nanocrystalline alloy and the technology of their synthesis [19]. For this reason considerable efforts have been made to search for nanocrystalline thin-film structures with high magnetization saturation and magnetic susceptibility, and low microwave losses [2,10,20–26].

One of the most important results, obtained during the investigation of nanocrystalline materials, was the establishment of a complex dependence of the magnetic microstructure, anisotropy, coercivity, and magnetic susceptibility on the grain size [7,27]. Currently, the random anisotropy model (RAM) originally proposed by Alben et al. [28] and subsequently modified by Herzer [29] is widely used to interpret this intricate dependence. According to this model, when the grain size is

---

* Corresponding author at: Siberian Federal University, 79 Svobodny pr., Krasnoyarsk 660041, Russia.
  E-mail address: psolovev@iph.krasn.ru (P.N. Solovev).

smaller than the exchange correlation length, the exchange coupling between grains leads to the averaging of the random anisotropy of individual grains resulting in a significant decrease of coercivity and increase in magnetic susceptibility of the nanocrystalline medium. Experimental studies support the validity of RAM not only for single-phase materials but also for multiphase and granular materials [30].

Because RAM is based on simple and clear concepts, this model is extensively used to interpret the soft magnetic properties of bulk materials as well as two-dimensional nanocrystalline thin films and multilayers [30–33]. Despite a convincing argument in the RAM theory, it can be used only for a qualitative but not quantitative analysis of the static properties of nanocrystalline thin films. In thin films, the dipolar interaction between grains, which is neglected in RAM, leads to the transformation of the shape and size of the region over which the averaging of the random anisotropy occurs [34]. The dipolar interaction also results in the formation in the film of inhomogeneous demagnetizing fields [35]. Specifically, the dipolar interaction together with the exchange interaction leads to the appearance of an inhomogeneous stochastic magnetic structure, called magnetization ripple. Magnetization ripple in nanocrystalline films is a well-established experimental fact [36] but it cannot be explained in the framework of RAM.

A more complete theoretical model, which takes into account both exchange and dipolar interactions between grains in thin films was considered by Hoffmann [34,35], Harte [37] Ignatchenko [38] back in the late 1960s in the framework of the magnetization ripple theory. Due to the long-range nature of the dipolar interaction [39] the micromagnetic problem of the grain size effect on the static and high-frequency properties of nanocrystalline thin films cannot be solved rigorously. Therefore, analytical expressions relating the microcrystalline structure of the film with its macroscopic magnetic characteristics were obtained within the magnetization ripple theory using some approximations. Today, the following questions are still relevant: (i) How justified are the approximations used in the magnetization ripple theory? and (ii) What are the limits of applicability of the analytical expressions?

Recent advances in numerical methods of the micromagnetic simulation and a significant increase in the computational power of modern computers have made it possible to investigate various complex magnetic structures with high accuracy [39]. To date, the micromagnetic simulation has become a standard, extensively used efficient tool that can provide an in-depth understanding of the magnetic behavior of ferromagnets, thin films in particular. For instance, numerical micromagnetic simulation of thin films have made it possible to study the magnetic microstructure and its correlation characteristics [40–42], as well as the influence of the structural [42–44] and technological [45,46] parameters on the coercivity and remanence. On the other hand, the simulation of the high-frequency response of nanocrystalline thin films is not so common [47,48] due to the significant computational difficulties [49]. In this paper, using micromagnetic simulation, we study in detail the influence of the grain sizes on the magnetic microstructure and high-frequency susceptibility of nanocrystalline thin films with the main focus on the investigation of the causes that lead to the ferromagnetic resonance line broadening.

2. Numerical simulations

2.1. Justification of the numerical model

A typical nanocrystalline thin magnetic film is a two-dimensional array of randomly oriented crystallites (grains) less than 100 nm in size, embedded in an amorphous magnetic matrix [50]. The average size D_0 and magnetocrystalline anisotropy constant K of grains are one of the most important parameters that determine the macroscopic magnetic properties of the films. However, the intergranular amorphous phase (with a typical thickness of about 1 nm) plays an equally important role by implementing the exchange coupling between grains [50].

Experiments show that the Curie temperature T_{cam} of an amorphous phase is substantially lower than that of a nanocrystalline phase indicating that the amorphous phase has a lower value A_{am} of the exchange constant than that of grains [7,30,50]. When the operating temperature exceeds T_{cam} or the composition of the nanocrystalline alloy is not optimized and $A_{am} = 0$, the magnetic coupling between grains is broken and the soft magnetic properties degrade correspondingly.

Nanocrystalline materials are one of the most complicated objects from the point of view of numerical micromagnetic simulations [49,51]. Since the magnetic anisotropy of individual grains is distributed randomly throughout the film, the magnetization processes and magnetization dynamics of such an inhomogeneous film can be studied only statistically. Therefore, in order to obtain valid and relevant simulation results, it is necessary to consider a large (statistically significant) number of grains in the model. Moreover, it should be taken into account that in real nanocrystalline materials the grains have a Gaussian size distribution, and the boundaries between crystalline and amorphous phases are complicated curved surfaces. This, in turn, imposes additional requirements to the discretization level of the considered object. Simultaneous satisfaction of all these requirements is not possible due to the existing limitations of computing power. Therefore, a balanced approach for simplifying the numerical model of a nanocrystalline thin film is required.

First, it was shown (see, for example, Ref. [30,50]) that in the framework of RAM, multiphase (including two-phase) magnetic systems for most nanocrystalline alloys can be considered as single-phase ones given that the model parameters were renormalized correspondingly. Such systems are described by effective (averaged) model parameters: average effective grain size D_0, effective local magnetocrystalline anisotropy constant K, effective exchange coupling constant $A \approx A_{am}$. In this paper, we limited ourselves to considering only the single-phase film model, hence, we did not study the effect of the real microstructure on the magnetic properties of nanocrystalline thin films.

Second, it is important to take into account that the magnetic moments inside the grain are coupled by exchange more strongly than the moments of neighbor grains, whose coupling mainly occurs via a thin amorphous interlayer. In addition, in this paper, we did not consider the magnetization reversal processes. We studied the magnetic microstructure and high-frequency properties of the films on a reversible part of the hysteresis loop. As it will be evident from the simulations results, the grain sizes considered in the model is sufficiently smaller than the radius of magnetic correlations (exchange and dipolar) within which the magnetization is almost uniform. These conclusions give us reason to consider individual grains as magnetically coupled uniformly-magnetized Stoner–Wohlfarth particles, that is, we use the macrospin approximation [52,53].

2.2. Micromagnetic model and calculation methods

To investigate the effect of grain size on the magnetic microstructure and high-frequency susceptibility of a nanocrystalline thin film, we used the following numerical micromagnetic model. Within the finite-difference method [39] the film was discretized on N identical cells of volume V_0. Each cell corresponded to an individual uniformly magnetized grain with the magnetic moment $\boldsymbol{\mu}_i = V_0 \, \mathbf{M}_i$, $(i = 1,2,..,N)$. It was assumed that for all grains, the modulus of the magnetization vectors $\mathbf{M}_i$ was constant and equal $M_s = |\mathbf{M}_i|$. Then the expression for the free energy F of the film is [44]

$$F = -V_0 \sum_{i=1}^{N} \left[\boldsymbol{HM}_i - \frac{A}{D_0^2} \sum_{\substack{j=1 \\ j \neq i}}^{Ni} \left(1 - \frac{\boldsymbol{M}_i \boldsymbol{M}_j}{M_s^2}\right) + \frac{1}{2} \sum_{j=1}^{N} \boldsymbol{M}_i G_{ij}^m \boldsymbol{M}_j + \frac{K}{M_s^2} (\boldsymbol{M}_i \boldsymbol{l}_i)^2 \right]$$

(1)

In this expression, the first term describes the energy of an external

magnetic field **H** (the Zeeman energy). The second term describes the energy of the exchange interaction between grains, where the inner summation is performed only over the nearest N_i neighbors of the ith grain. The third term describes the energy of the demagnetizing fields, where $G_{ij}^m \in \mathbf{R}^{3\times3}$ is a 3×3 tensor, which describes the magnetostatic or dipolar interaction between grains i and j [44]. Finally, the last term of the expression represents the energy of the uniaxial magnetic anisotropy K with a random orientation of magnetization easy axes $\mathbf{l}_i$ in the grains. Expression (1) can be rewritten in a more convenient and compact form

$$F = -V_0 \sum_{i=1}^{N} \left[\boldsymbol{HM}_i + \frac{1}{2} \sum_{j=1}^{N} \boldsymbol{M}_i G_{ij} \boldsymbol{M}_j \right], \tag{2}$$

where G_{ij} is an effective 3×3 tensor describing interactions between grains i and j. The tensor G_{ij} does not depend on the magnetization orientation $\mathbf{M}_i$, it is determined solely by the intrinsic properties of the investigated magnetic system, $G_{ij} = G_{ij}^e + G_{ij}^m + G_{ij}^a$. Here $G_{ij}^e \in \mathbf{R}^{3\times3}$ is a tensor describing exchange interaction, and $G_{ij}^a \in \mathbf{R}^{3\times3}$ random uniaxial magnetic anisotropy. The elements of the symmetric tensors which represent the exchange interaction and magnetic anisotropy are given by

$$G_{ij}^e = \frac{2A}{M_s^2 D_0^2} E, \text{ (for the nearest neighbors } i \text{ and } j), \ G_{ij}^a = \frac{2K}{M_s^2} l_i \otimes l_j \delta_{ij}, \tag{3}$$

where E is an identity matrix of size 3×3, the sign $\otimes$ means tensor product, and δ_{ij} is the Kronecker delta.

The magnetic behavior of the medium is determined by the effective magnetic field acting on each grain

$$\boldsymbol{H}_i^{eff}(\boldsymbol{M}_1, ..., \boldsymbol{M}_N) = -\frac{1}{V_0} \frac{\delta F}{\delta \boldsymbol{M}_i} = \boldsymbol{H}_i + \sum_{j=1}^{N} G_{ij} \boldsymbol{M}_j. \tag{4}$$

If we divide the magnetization and the effective magnetic field on the static and dynamic parts $\boldsymbol{M}_i = \boldsymbol{M}_{0i} + \boldsymbol{m}_i(t)$, $\boldsymbol{H}_i^{eff} = \boldsymbol{H}_{0i}^{eff} + \boldsymbol{h}_i^{eff}(t)$, the equilibrium magnetization $\mathbf{M}_{0i}$ of the ith grain can be found from the condition $[\boldsymbol{M}_{0i} \times \boldsymbol{H}_{0i}^{eff}] = 0$, or, as was shown in Ref. [44] from the system of linear inhomogeneous equations with undetermined Lagrange multipliers ν_i

$$\boldsymbol{H}_{0i}^{eff}(\boldsymbol{M}_{01}, \boldsymbol{M}_{02}, ..., \boldsymbol{M}_{0N}) - \nu_i \boldsymbol{M}_{0i} = 0, \quad (i = 1, ..., N) \tag{5}$$

According to Eqs. (4) and (5), the static and dynamic parts of the effective field are given by

$$\boldsymbol{H}_{0i}^{eff} = \sum_{j=1}^{N} G_{ij} \boldsymbol{M}_{0j} + \boldsymbol{H}_0 = \nu_i \boldsymbol{M}_{0i}, \quad \boldsymbol{h}_i^{eff}(t) = \sum_{j=1}^{N} G_{ij} \boldsymbol{m}_j(t) + \boldsymbol{h}^{rf}(t), \tag{6}$$

where $\mathbf{h}^{rf}(t)$ is the external high-frequency magnetic field.

To solve the system of inhomogeneous equations (5), we used an approach based on the system relaxation according to the internal effective magnetic fields acting on each magnetic moment [44]. At each iteration step, the effective local magnetic field was calculated, and a new distribution of magnetization was set in the direction of the acting force. The iterative process continued until the position of all magnetic moments were stabilized within a given accuracy. It is important to note that the obtained equilibrium magnetization distribution was checked for stability, and if this test was failed, the new search for the equilibrium distribution in the direction of system relaxation was launched [44].

To investigate the dynamic behavior of the nanocrystalline thin magnetic films, we used the linearized system of Landau–Lifshitz equations. As was shown in Ref. [49] this system can be written as

$$\frac{\partial \boldsymbol{m}_i}{\partial t} = \sum_{j=1}^{N} B_{ij} \boldsymbol{m}_j + N_i \boldsymbol{h}^{rf}, \quad (i = 1, ..., N) \tag{7}$$

The following notation was used

$$N_i = -\gamma \left(\Lambda(\boldsymbol{M}_{0i}) + \frac{\alpha}{M_s} (\Lambda(\boldsymbol{M}_{0i}))^2 \right), \quad \Lambda(\mathbf{M}_{0i})$$

$$B_{ij} = N_i \left(G_{ij} - \nu_i \delta_{ij} E \right)$$

$$\equiv \begin{pmatrix} 0 & -M_{0i}^{(z)} & M_{0i}^{(y)} \\ M_{0i}^{(z)} & 0 & -M_{0i}^{(x)} \\ -M_{0i}^{(y)} & M_{0i}^{(x)} & 0 \end{pmatrix}, \tag{8}$$

where $\gamma = 1.76 \times 10^7$ rad/s Oe is the gyromagnetic ratio, and α is a dimensionless damping parameter.

We used the numerical realization of the undetermined coefficients method to solve the linearized Landau–Lifshitz equations system. This numerical approach was described in detail in our previous paper [49]. By substituting $\boldsymbol{m}_i(t) = \boldsymbol{m}_{0i} e^{-i\omega t}$ and $\boldsymbol{h}^{rf}(t) = \boldsymbol{h}_0 e^{-i\omega t}$, the system of differential equations (7) is reduced to the system of linear inhomogeneous equations

$$-i\omega \boldsymbol{m}_{0i} = \sum_{j=1}^{N} B_{ij} \boldsymbol{m}_{0j} + N_i \boldsymbol{h}_0, \quad (i = 1, ..., N), \tag{9}$$

that can be solved by using standard numerical methods of linear algebra [49].

After determination of the dynamic magnetization amplitude $\mathbf{m}_{0i}$, the magnetic susceptibility χ of a nanocrystalline thin film was determined from the expression

$$\chi = \frac{1}{N} \sum_{i=1}^{N} \frac{\boldsymbol{m}_{0i} \cdot \boldsymbol{h}_0}{|\boldsymbol{h}_0|^2} \tag{10}$$

As shown in Ref. [49] the undetermined coefficients method has a much lower computational complexity in comparison with the method based on the expansion of the solution of the linearized Landau–Lifshitz equation in terms of eigenvectors of the magnetic oscillation modes.

2.3. Modeling details

The investigated films were monolayers of close-packed grains having the randomly oriented axes of uniaxial anisotropy (local anisotropy). The number of grains used in the model was $N = 1024 \times 1024 \times 1$. The size of each grain D_0 coincided with the size of the discrete cell and varied in the range 12–100 nm. To eliminate the effect of grain shape anisotropy on the simulation results, we chose a cubic shape for the discrete cells. The volume of the cell corresponded to the average volume of the grain, $V_0 = D_0^3$. Therefore, the thickness d of the investigated monolayer film equaled D_0. The components of the tensor that describe the dipolar interaction between grains were calculated using an analytical expression obtained in Ref. [54]. We applied two-dimensional periodic boundary conditions for the exchange and dipolar interactions [55] to eliminate the edge effects originating from inhomogeneity of an internal magnetic field in samples of finite size [56].

For concreteness, magnetic parameters of the investigated films were chosen to correspond to a well-known nanocrystalline alloy $Fe_{73.5}Cu_1Nb_3Si_{13.5}B_9$ [27]: the saturation magnetization $4\pi M_s = 12$ kG (1.2 T), the effective exchange constant $A = 1 \times 10^{-6}$ erg/cm (1×10^{-11} J/m), the damping parameter $\alpha = 0.005$. We defined the random magnetic anisotropy of the film by assigning to each grain the uniaxial magnetic anisotropy field and the orientation of the easy axis. For all grains, the anisotropy field was the same, $H_k = 2 K/M_s = 171.7$ Oe ($K = 8200$ J/m³), while the orientations of the easy axes $\mathbf{l}_i$ ($i = 1,2,..,N$) were random. We note that the orientation of the easy axis $\mathbf{l}_i$ varied randomly from grain to grain, satisfying to the following uniform distribution function of the vector $\mathbf{l}$ in a spherical coordinate system: $f(\mathbf{l}) = f(\theta,\varphi) = \sin\theta/4\pi$, where θ and φ are the polar and azimuthal angles of the vector

1.

The mutually perpendicular external constant **H** and alternating $\mathbf{h}^{rf}(t)$ uniform magnetic fields were applied in the film plane. In Table 1 we additionally show the ratio between the exchange energy $F^e = -VA/D_0^2$ and energy of the randomly oriented local anisotropy $F^a = -VK$, where V is the film's volume.

3. Numerical results and discussion

3.1. Magnetic microstructure

The main feature of nanocrystalline thin magnetic films is the small size of crystallites in comparison with the correlation radius of the exchange and dipolar interactions. The magnetic coupling between crystallites leads to the averaging and partial suppression of the local magnetic crystalline anisotropy. However, usually local anisotropy does not average out completely. Because of that, the film exhibits small fluctuations of the magnetization vector from its spatial average direction. This stochastic micromagnetic structure is known as magnetization ripple [34,35,37,38].

In magneto-optical experimental studies on magnetization ripple, when a sample is magnetized along the *x*-axis, the intensity of the reflected light is proportional to the transversal component of the magnetization M_y [57]. For the corresponding geometry, Fig. 1 shows numerically calculated distributions of the reduced transversal magnetization component $m_y = M_y/M_s$, over the film surface for the applied external field $H = 10$ Oe and $D_0 = 12, 24, 42, 75$ nm. Here, both the constant magnetic field **H** and the average magnetization $< \mathbf{M}_i >$ are oriented along the *x*-axis. The stages of the transversal component m_y transformation with the variation of the applied field are shown in Fig. 2 for the film with $D_0 = 24$ nm. The color in these figures corresponds to the magnitude of the magnetization deviation to the right and left from its average direction. The calculated distributions reveal the appearance of magnetization ripple and agree well with the images of magnetization configuration in nanocrystalline films obtained with Kerr microscopy [57].
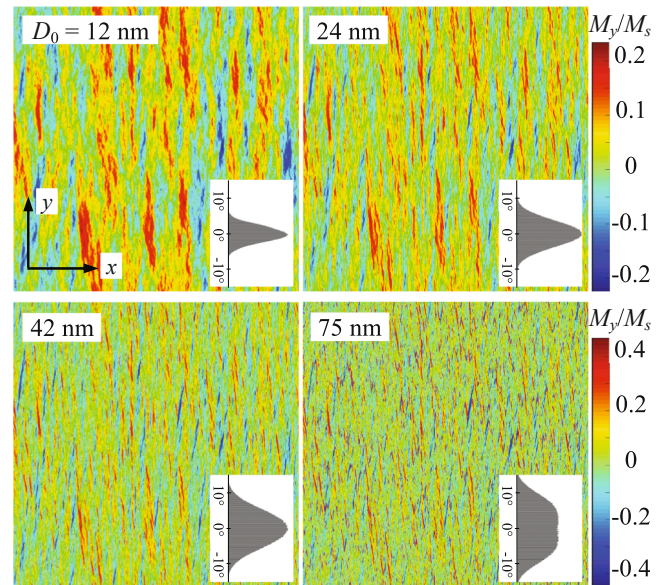
Insets in Figs. 1 and 2 additionally show the distributions of the magnetic moments of individual grains depending on the angle of their deviation from the average magnetization (that lies along the *x*-axis). As it follows from these figures, with the increase of the grain size D_0, the magnetic correlations (the size of the regions coupled by the exchange and dipolar interactions) decrease, while the amplitude of the magnetization fluctuations increases. A somewhat different picture is observed when the value of the external magnetic field changes. With the increase of the applied constant field H, the size of the magnetic correlations also decreases. But, as can be seen from the insets in Fig. 2, the amplitude of the magnetization fluctuations reduces significantly indicating that the magnetization of the film approaches saturation.

The most rigorous and consistent static theory of magnetization ripple was developed by Hoffmann [34,35]. Hoffmann, following the results of electron microscopy studies, introduced a model of magnetically coupled regions formed in the film that do not interact with each other. The size and shape of such regions depend on the radius of the exchange and dipolar interactions, grain size, and the magnitude of the applied field. Generally, this magnetically coupled region is an ellipsoid strongly elongated perpendicular to the mean direction of the magnetization. The lengths of the major semiaxis $R_\perp$ (perpendicular to the

Fig. 1. Calculated distributions of the reduced transversal magnetization component $m_y = M_y/M_s$ in a thin film for four grain sizes $D_0 = 12, 24, 42, 75$ nm. Applied constant magnetic field $H = 10$ Oe. Insets show the distribution of the magnetic moments depending on the angle of their deviation from the *x*-axis. The applied constant field and the average magnetization are oriented along the *x*-axis.
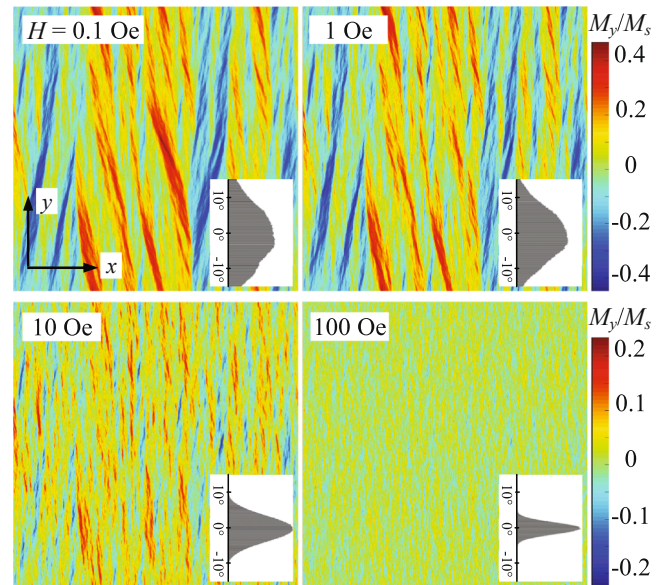
Fig. 2. Calculated distributions of the reduced transversal magnetization component $m_y = M_y/M_s$ in a thin film for four values of the applied field H. The grain size $D_0 = 24$ nm. Insets show the distribution of the magnetic moments depending on the angle of their deviation from the *x*-axis. The applied constant field and the average magnetization are oriented along the *x*-axis.

mean direction) and minor semiaxis $R_\parallel$ (parallel) in the linear approximation are given by [34].

$$R_\parallel = \sqrt{D/H}, \quad R_\perp = 4\sqrt{d}D^{1/4}M_s^{1/2}H^{-3/4}, \tag{11}$$

where $D = 2A/M_s$. Averaging magnetic anisotropy of randomly oriented crystallites within the magnetically coupled region, Hoffmann obtained the following expression for the dispersion of the transverse magnetization component
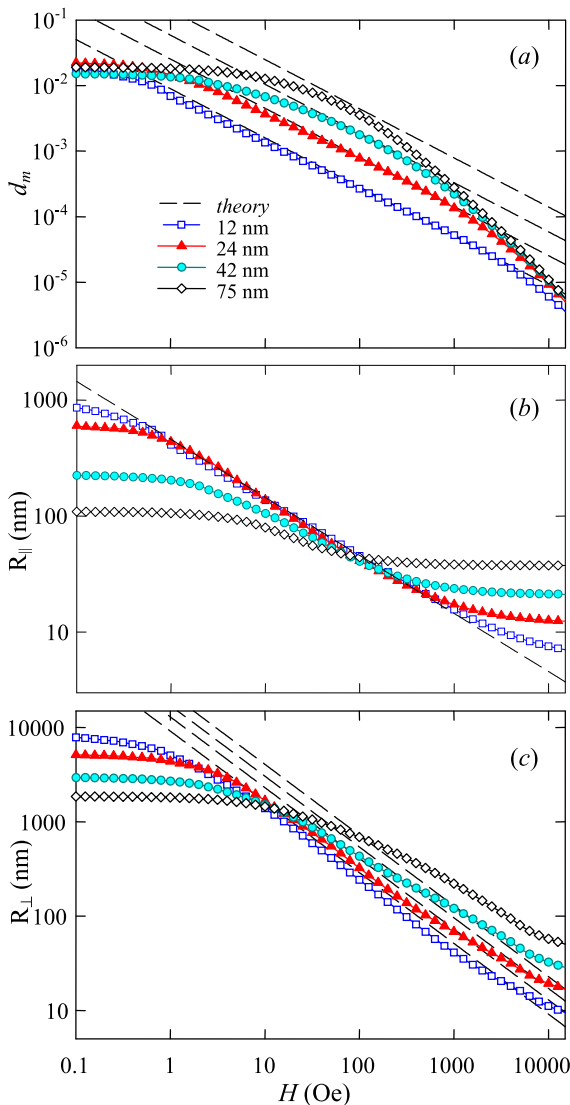
Table 1
The ratio between the exchange energy F^e and the energy of the randomly oriented local anisotropy F^a of nanocrystalline thin magnetic films for different grain sizes D_0.

D_0	12 nm	24 nm	32 nm	42 nm	56 nm	75 nm	100 nm
F^e/F^a	8.47	2.12	1.19	0.69	0.39	0.22	0.12
F^a/F^e	0.12	0.47	0.84	1.45	2.57	4.61	8.2

$$d_m = <m_y^2> = \frac{S^2}{4\pi\sqrt{d}M_s^{10/4}D^{3/4}H^{3/4}} \qquad (12)$$

The expression (12) includes structural constant S that was introduced by Hoffmann for a quantitative description of the magneto-structural properties of the film. The structural constant is defined as $S = D_0 K \sigma_1 / \sqrt{n}$, where σ_1 is a constant that characterizes the rms deviation of the easy magnetization axes of crystallites ($\sigma_1 = 2/\sqrt{15}$ for uniaxial anisotropy, $\sigma_1 = \sqrt{8/105}$ for cubic anisotropy), and n is a number of grains over the film thickness.

We estimated the magnetization dispersion and the size of the magnetically coupled regions on the calculated distributions by using the correlation function for the reduced magnetization component m_y

$$K_m(r) = <m_y(r')m_y(r'+r)> . \qquad (13)$$

The value of the correlation function at $r = 0$ determines the magnetization dispersion, that is $d_m = K_m(0)$. The magnetic correlation radiuses along $R_\parallel$ and transverse $R_\perp$ to the mean direction of the magnetization were determined from the function $K_m(r)$ as a distance (along the corresponding direction) at which the correlations decrease by a factor of $e \approx 2.718$, that is, from the condition $K_m(R_{\parallel,\perp}) = K_m(0)/e$. Fig. 3 shows the dispersion d_m and longitudinal $R_\parallel$ and transverse $R_\perp$ correlation radiuses versus the applied magnetic field, calculated from the correlation analysis of the equilibrium magnetization distribution for the films with $D_0 = 12, 24, 42, 75$ nm. The dashed lines on the plots display theoretical dependences of these parameters, calculated using formulas (11) and (12).

One can see that the ripple theory of Hoffmann is in better agreement with the simulation results the smaller the grain size is used in the calculation. In the range of the large magnetic fields, the observed differences are due to the fact that the further decrease of the size of the magnetically coupled region with the increase of H is limited by the size of the grains. This was noted by Harte [37] who instead of (11) used the approximation $R_\parallel \approx \sqrt{D/H}+R$ for the case when the exchange correlation length $\sqrt{D/H}$ was comparable with the grain radius $R = D_0/2$. In agreement with this approximation, the longitudinal correlation radius $R_\parallel$, obtained from the micromagnetic simulation, tends to R for $H \to \infty$ (Fig. 3b). In the weak fields region, the results of the micromagnetic simulation and theory are also in disagreement. In this case, the ratio between the value of the applied field and magnetic parameters of the sample is such that the linear approximation used by Hoffmann for deriving expressions (11) and (12) is no longer valid. As was shown by Harte [37] and subsequently by Hoffmann [34] if the rms deviation of the magnetization direction $<\phi> \approx \sqrt{d_m}180/\pi$ is larger than $1°–2°$, then it is necessary to consider in the theoretical model the effect of nonlinear terms of the equilibrium magnetization equation.

These results are also in good agreement with the experimental data reported by other authors. Iskhakov et al. [58] measured the dispersion d_m of the transversal magnetization component as a function of an applied magnetic field for the nanocrystalline 10-nm-thick $Co_{93}P_7$ film. As in our numerical model, the grain size of the nanocrystalline alloy $Co_{93}P_7$ was about the film thickness. The authors showed that in the field range $0.2 \div 2$ kOe, $d_m \sim H^{-3/4}$, in agreement with the expression (12) and simulation results shown in Fig. 3. Michels et al. [59] directly measured magnetic correlations in a nanocrystalline Co film employing small-angle neutron scattering (SANS). The mean grain size of the Co film was 10 nm, although the thickness of the film was 160 μm. The authors approximated the experimental dependence of the magnetic correlation length by the dependence $R_\parallel \sim \sqrt{D/H} + D_0$, which again agrees quite well with our simulation results. The authors also measured the dependence of the dispersion d_m on the applied field. They approximated this dependence as $d_m \sim H^{-1}$. However, a careful analysis of the experimental dependence $d_m(H)$ presented in the paper [59] allows us to draw a reasoned conclusion that $d_m \sim H^{-3/4}$ would be the better approximation in the wide range ($1 \div 10^3$ mT) of internal magnetic field.

Fig. 3. Dispersion d_m (a), longitudinal $R_\parallel$ (b) and transverse $R_\perp$ (c) correlation radiuses of the reduced magnetization component $m_y = M_y/M_s$ versus the applied magnetic field H for several values of D_0. Symbols are micromagnetic simulation, dashed lines are theoretical calculations according to the expressions (11) and (12).
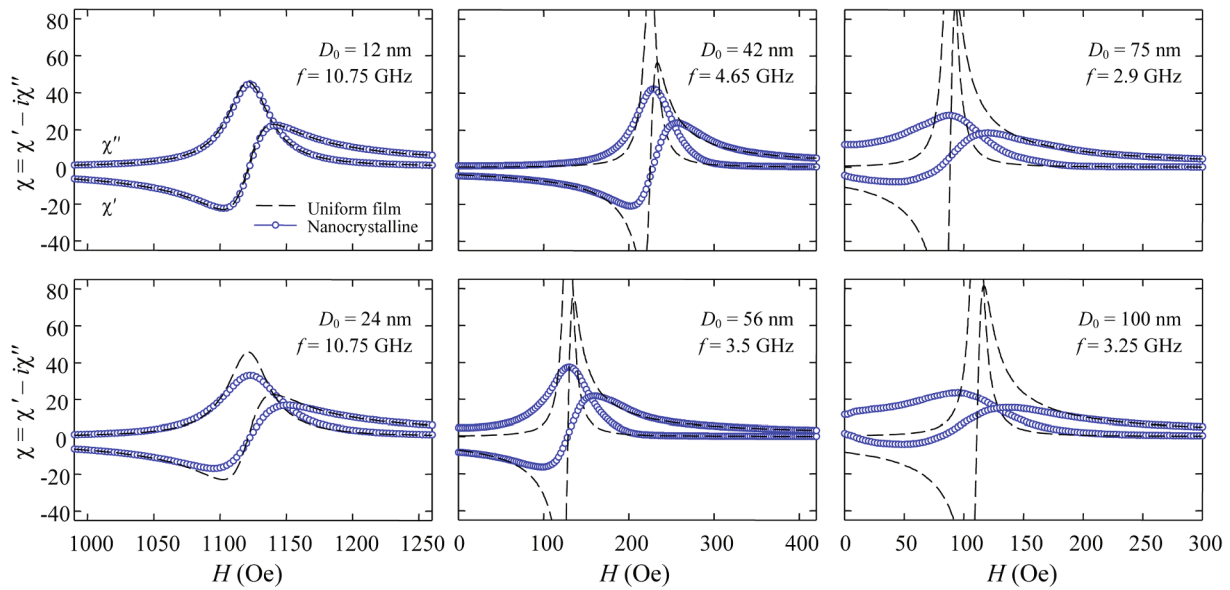
3.2. High-frequency susceptibility

The phenomenological theory of ferromagnetic resonance in an isotropic uniformly magnetized thin film gives the following simple expression for the magnetic susceptibility [60]

$$\chi(H) = \chi' - i\chi'' = \frac{1}{4\pi} \frac{\omega_M(\omega_M + \omega_H)}{\omega_0^2 - \omega^2 + i\alpha\omega(\omega_M + 2\omega_H)}, \qquad (14)$$

where $\omega_M = \gamma 4\pi M_s$, $\omega_H = \gamma H$, $\omega_0 = 2\pi f_0 = \sqrt{\omega_H(\omega_M + \omega_H)}$ is the frequency of the uniform FMR, and $\omega = 2\pi f$ is the frequency of the applied alternating magnetic field.

The random local anisotropy in nanocrystalline thin films can substantially affect their high-frequency susceptibility behavior [47,49]. This is confirmed by the results of $\chi(H)$ calculations presented in Fig. 4. The dashed lines on this figure show real $\chi'(H)$ and imaginary $\chi''(H)$ parts of the susceptibility calculated using expression (14), while

Fig. 4. The field dependences of the high-frequency magnetic susceptibility $\chi(H)$ for nanocrystalline films of various grain sizes $D_0 = 12, 24, 42, 56, 75, 100$ nm, obtained at the frequencies of the maximum broadening of the FMR line (symbols). The dashed lines correspond to $\chi(H)$ of the uniformly magnetized films (equation (14)).

symbols show the results of the numerical simulation. The dependences on Fig. 4 were obtained for the several values of frequencies of the alternating applied field $f = f_1 = 10.75, 4.65, 3.5, 2.9, 3.25$ GHz, at which in the films with $D_0 = 24, 42, 56, 75, 100$ nm the maximum broadening of the FMR line was observed. As will be shown below, for the film with $D_0 = 12$ nm the FMR line broadening increases monotonically with f and does not have any noticeable maximum. Because of that, for this sample as well as for the film with $D_0 = 24$ nm, the dependence $\chi(H)$ was obtained for $f = 10.75$ GHz (Fig. 4).

It is apparent from the results shown in Fig. 4, that for the films with the ratio F^e/F^a greater than 1, the exchange interaction between crystallites greatly suppresses the local anisotropy influence. This is notably for the film with $D_0 = 12$ nm, where the exchange energy more than eight times larger than the energy of the local anisotropy (Table 1). The magnetic characteristics of this film are close to that of an isotropic uniformly magnetized film, and its field dependence of the magnetic susceptibility is almost identical to the curve obtained using expression (14). With the increase of the grain size, however, the local anisotropy energy begins to dominate over the exchange energy, leading to the substantial broadening and asymmetry in $\chi''(H)$ line and also to the shift of the resonance field. If the grain size is comparable to the exchange correlation length, then the magnitude of the magnetization spatial fluctuations rises drastically. This is the case for the film with $D_0 = 100$ nm, for which the local anisotropy energy is at least eight times larger than the exchange energy. As can be seen from Fig. 4, for this film the $\chi(H)$ dependence deviates from the behavior of the uniformly magnetized film most strongly.

3.3. Resonance field shift and FMR line broadening

The FMR linewidth of any magnetic material is determined by a number of relaxation mechanisms of different nature. These mechanisms are usually divided into two broad classes – intrinsic, that present even in an ideal crystal, and are taken into account phenomenologically by the damping parameter α, and extrinsic [60]. The latter contribution arises due to the presence of inhomogeneities in the material. Among the extrinsic relaxation mechanisms, the two-magnon scattering processes are of most importance. According to the two-magnon model, the energy of the excited uniform FMR mode might scatter on internal inhomogeneous magnetic fields to the degenerative spin wave states. These

inhomogeneous fields (scattering centers) may originate from various sources. For instance, the authors of Refs. [48,61] analyzed the influence of the randomly oriented local anisotropy on the two-magnon scattering processes in polycrystalline thin films, whereas the effect of randomly distributed roughnesses on the surface of the film was studied in Refs. [62,63].

To divide intrinsic and extrinsic contributions to the relaxation, we can write the resonance field H_R and FMR linewidth ΔH obtained from the micromagnetic simulation, as a sum consisting of two parts

$$H_R = H_0 + H^{(2m)},$$
$$\Delta H = \Delta H_0 + \Delta H^{(2m)}, \tag{15}$$

where the first term on the right side of each expression includes only intrinsic relaxation mechanism and corresponds to the uniform FMR of a thin film, while the effects from the two-magnon scattering processes are taken into account in the second term. The resonance field H_0 should satisfy the condition $\omega_0 = 2\pi f_0 = \sqrt{\omega_H(\omega_M + \omega_H)}$, and at resonance frequencies f_0 lower than 10–15 GHz, can be approximated as $H_0 \approx \pi(f_0/\gamma)^2/M_s$. The linewidth of the uniform FMR is determined by the well-known expression $\Delta H_0 = 4\pi\alpha f_0/\gamma$ [60].

According to the theory of the two-magnon scattering processes developed by Arias and Mills for the inhomogeneous ultrathin films [63] the frequency dependence of the FMR line broadening $\Delta H^{(2m)}$ is given by

$$\Delta H^{(2m)} = \Gamma arcsin \frac{H_0}{H_0 + 4\pi M_s} = \Gamma arcsin \sqrt{\frac{\sqrt{f_0^2 + (f_M/2)^2} - f_M/2}{\sqrt{f_0^2 + (f_M/2)^2} + f_M/2}}, \tag{16}$$

that is commonly used to interpret experimental dependencies $\Delta H(f_0)$ [64–66]. Here $f_M = \omega_M/2\pi$, and Γ is a frequency-independent constant that characterizes the "intensity" of magnetic inhomogeneities. As it follows from (16), the $\Delta H^{(2m)}$ monotonically increases with f_0 without any peculiarities.

However, our micromagnetic simulation results show that nanocrystalline thin films can exhibit a sharp peak in the FMR linewidth at a certain frequency f_1. This peak emerges only when the grain size D_0 exceeds a certain threshold value. As an example, in Fig. 5a we show dependencies $\Delta H^{(2m)}(f_0)$ obtained by the micromagnetic simulation of
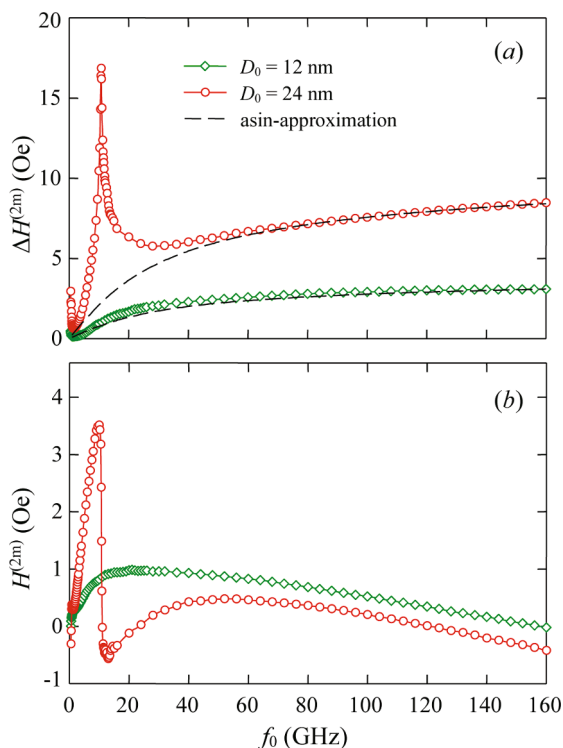
Fig. 5. The frequency dependencies of the FMR line broadening $\Delta H^{(2m)}$ (*a*) and resonance field shift $H^{(2m)}$ (*b*), obtained by the micromagnetic simulation of the high-frequency susceptibility for the films with grain sizes $D_0 = 12$ and 24 nm. The dashed lines are approximations according to equation (16).
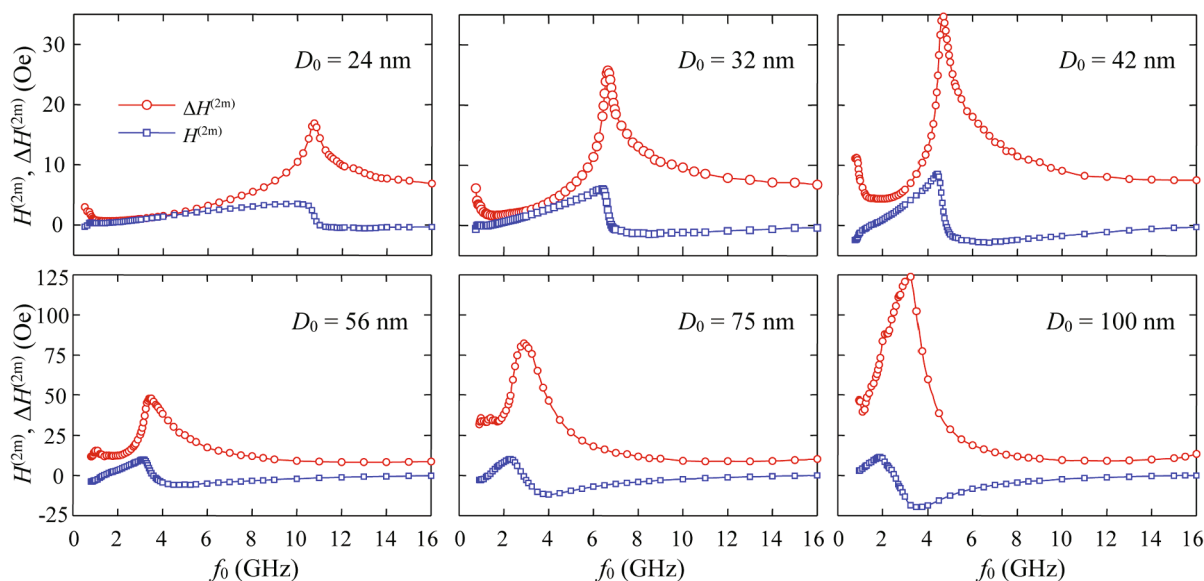
high-frequency susceptibility for the films with $D_0 = 12$ and 24 nm. The dashed lines on the figure show the approximation of the dependencies $\Delta H^{(2m)}(f_0)$ according to the equation (16). The theory of Arias and Mills is in quite good agreement with the results of micromagnetic simulation for the film with the relatively small grains $D_0 = 12$ nm and the thickness $d = D_0$. On the contrary, for the film with $D_0 = 24$ nm, the micromagnetic simulation gives a sharp peak in the FMR linewidth $\Delta H^{(2m)}$ at the frequency of $f_1 \approx 10.75$ GHz, while at higher frequencies the simulation and theory are in accord again.

The broadening of the FMR line by the value of $\Delta H^{(2m)}$ due to the two-magnon scattering mechanism is also accompanied by the shift of the resonance field by the value $H^{(2m)}$, relative to the field H_0 of the uniform ferromagnetic resonance. This is evident from Fig. 5b, where the dependencies $H^{(2m)}(f_0)$ calculated for the films with $D_0 = 12$ and 24 nm are shown. For the film with $D_0 = 12$ nm, the resonance field shift $H^{(2m)}$ initially gradually increases with the increase of the resonance frequency f_0, reaches a maximum of 1 Oe at a frequency of 21 GHz, and then monotonically decreases down to zero at a frequency of 160 GHz. However, the film with $D_0 = 24$ nm behaves quite differently. The sharp increase in the linewidth comes together with the substantial positive and negative shift of the resonance field. It is noticeable that $H^{(2m)}$ changes sign approximately at the frequency position ($f_1 \approx 10.75$ GHz) of the linewidth peak. It is interesting to note that the behavior of the dependencies $H^{(2m)}(f_0)$ and $\Delta H^{(2m)}(f_0)$, considered together, has features that are specific to resonance systems. Indeed, $H^{(2m)}(f_0)$ and $\Delta H^{(2m)}(f_0)$ bear a formal resemblance to real and imaginary parts of the resonance curve describing some "oscillation process".

With the increase of the grain size, the found resonance-like behavior of $\Delta H^{(2m)}(f_0)$ and $H^{(2m)}(f_0)$ retain (Fig. 6), and at the same time the two-magnon contribution to the linewidth quickly increases, while the frequency f_1 of the peak on the $H^{(2m)}(f_0)$ dependence monotonically decreases (Table 2). As can be seen from Table 2, the linewidth increases on about a factor of 1.5 for the films with $D_0 = 24$ nm and about 10 for films with $D_0 = 100$ nm. For each film in Table 2, we also show correlation characteristics of the magnetic microstructure formed in the film in an external magnetic field at which the uniform ferromagnetic resonance was observed at the frequency of f_1. The rms deviation of the magnetization from the mean direction $< \varphi >$ increases almost linear with the increase of the grain size, from $0.6°$ for $D_0 = 24$ nm to $4°$ for $D_0 = 100$ nm. This indicates that with the increase of D_0, the contribution to the relaxation processes from the internal inhomogeneous magnetic fields caused by the magnetization dispersion rises. Particularly, as one can see in Fig. 6, the magnetization dispersion leads to the distortion and "widening" of the $\Delta H^{(2m)}(f_0)$ and $H^{(2m)}(f_0)$ curves, and, as a consequence, to the shift of the linewidth peak frequency f_1.

3.4. Theoretical analysis of the FMR line broadening

The revealed with the help of the micromagnetic simulation resonance-like behavior of the FMR linewidth and resonance field shift

Fig. 6. The frequency dependencies of the resonance field shift $H^{(2m)}$ (blue squares) and FMR line broadening $\Delta H^{(2m)}$ (red circles) obtained by the micromagnetic simulation of high-frequency magnetic susceptibility for nanocrystalline films with grain sizes $D_0 = 24, 32, 42, 56, 75, 100$ nm. The thickness of the films is $d = D_0$.

Table 2

The frequency f_1 of the FMR linewidth peak caused by the two-magnon scattering on magnetization ripple and the broadening magnitude $\Delta H^{(2m)}$ versus grain size D_0. Also shown the resonance field H_0 and linewidth ΔH_0 of the uniformly magnetized film. For the corresponding values of D_0 and H_0, the table gives the correlation characteristics of magnetization ripple—dispersion d_m, rms deviation $<\phi> \approx \sqrt{d_m} 180/\pi$, and longitudinal $R_\parallel$ and transverse $R_\perp$ correlation radiuses of the magnetization component $m_y = M_y/M_s$.

D_0, nm	f_1, GHz	ΔH_{2m}, Oe	H_0, Oe	ΔH_0, Oe	$d_m \times 10^4$	$<\varphi>$, °	$2R_\parallel/D_0$	$2R_\perp/D_0$
24	10.75	16.9	1121	38.4	1.2	0.6	1.4	5.4
32	6.65	25.7	452	23.7	3.8	1.1	1.5	8.8
42	4.66	35.0	225	16.6	9.5	1.8	1.5	12.8
56	3.46	47.6	129	12.5	21.2	2.6	1.4	16.8
75	2.89	82.2	89	10.4	39.3	3.6	1.2	19.3
100	3.26	123.7	111	11.6	41.4	4.0	1.1	17.6

has been theoretically addressed by Ignatchenko and Degtyarev [67]. These authors were the first to devise the dynamic theory of magnetization ripple (see also a paper of Ignatchenko [38]). In the paper [67] they showed that the shift and asymmetric broadening of the FMR line is caused by the excitation of spin waves by an external uniform alternating field due to the inhomogeneities of the internal fields, originating from the random field of local magnetic anisotropy and magnetization ripple. Ignatchenko and Degtyarev also showed that the shift and broadening of the FMR line in such nonuniform films had a resonance-like character in the frequency dependencies. They obtained the following approximate formula for the determination of the frequency f_1, at which the broadening of the FMR line $\Delta H^{(2m)}$ has maximum and resonance field shift $H^{(2m)}$ changes sign
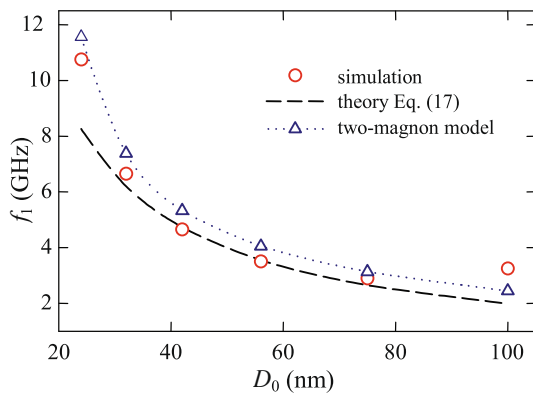
$$f_1 \approx 2\frac{\gamma}{d}\sqrt{\frac{A}{\pi}}\sqrt{\frac{d}{D_0}}. \tag{17}$$

The dependence of the frequency f_1 on the grain size, obtained from the micromagnetic simulation results, are presented in Fig. 7 (symbols). The dashed line on the figure displays the theoretical dependence $f_1(D_0)$, calculated according to expression (17) while taking into account that in the micromagnetic simulation the film thickness d equals the grain size D_0. One can see that the simulation and theoretical results are in reasonable agreement with each other.

Let us now consider a simple two-magnon model of FMR damping in a nanocrystalline thin film. This model makes it possible to clearly explain the revealed sharp FMR line broadening and the existence of the critical grain size below which this effect disappears. The spin-wave dispersion relation for a homogeneous isotropic thin film is given by [63]

$$\omega_k = \gamma\sqrt{[H + Dk^2 + 4\pi M_s N_k][H + Dk^2 + 4\pi M_s sin^2\phi_k(1 - N_k)]}. \tag{18}$$

Here, Dk^2 is the exchange field for a spin wave with wave vector $\mathbf{k}$ (k

$= |\mathbf{k}|$), φ_k is the angle between the spin wave propagation direction and the equilibrium magnetization, N_k is the demagnetization factor that depends on the wavenumber k and film thickness d. In the approximation of a thin film, in which the magnetization does not vary significantly across the thickness of the film, this factor can be written as [37]

$$N_k(k, d) = \frac{1 - e^{-kd}}{kd}. \tag{19}$$

Dispersion relation (18) is schematically shown in Fig. 8(a). In this figure, ω_0 shows the frequency of the uniform FMR mode with $k = 0$, and the curves with $\varphi_k = 0°$ and $\varphi_k = 90°$ correspond to the lower and upper limit of the spin-wave spectrum. One can see that dispersion curves with $\phi_k < \phi_k^{crit}$ cross the ω_0 line. This means that the frequency of the uniform FMR mode coincides with the frequencies of a set of spin waves having $0 < k_i < k_s$. Thus, the excitation of the uniform mode can result in the excitation of higher-order degenerate spin waves. However, as we have mentioned earlier, this is only possible if the film has magnetic inhomogeneities. As it was shown in Ref. [68,69], if the magnetic
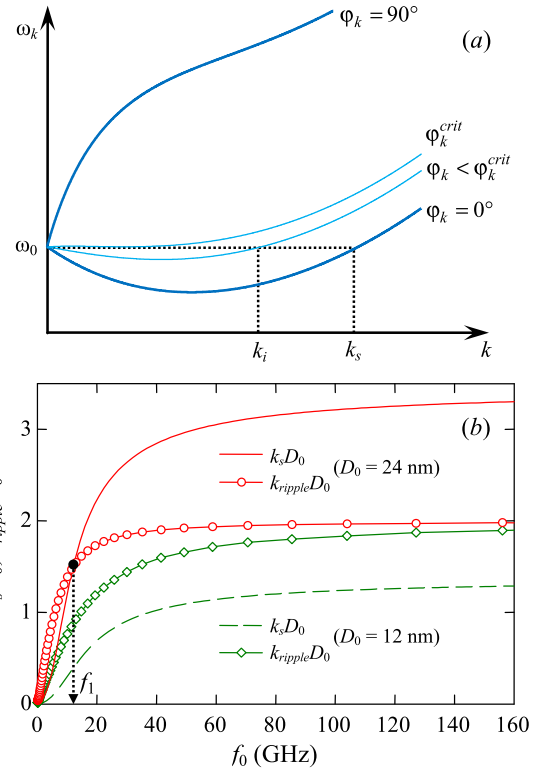
Fig. 7. The dependence of the linewidth peak frequency position f_1 on the grain size D_0. Circles are micromagnetic simulation, dashed line is the theoretical result according to equation (17), and triangles are the calculation using the two-magnon model of FMR damping.

Fig. 8. (a) Dispersion dependences of spin waves for different directions of their propagation φ_k in the film plane. (b) Maximum wavenumber of a degenerate spin wave k_s and wavenumber of magnetization ripple $k_{ripple} = 1/R_\parallel$ as a function of frequency $f_0 = \omega_0/2\pi$ for two values of grain sizes $D_0 = 12$ and 24 nm.

inhomogeneities are periodic in nature, then the energy of the uniform mode can be transferred to the spin waves most efficiently when the wavenumber of the periodic magnetic inhomogeneities is equal to or a multiple of the wavenumber of the degenerate spin wave.

Magnetization fluctuations arising in nanocrystalline thin films (magnetization ripple) induce quasi-periodic magnetic in-homogeneities. The characteristic size of these inhomogeneities along the spin wave propagation direction ($\varphi_k = 0°$) is determined by the longitudinal correlation radius $R_{||}$. It should be expected that the spin waves will scatter on these magnetic inhomogeneities most intensely when $k_s = k_{ripple}$, where $k_{ripple} = 1/R_{||}$. For a given value of ω_0, the maximum wavenumber k_s is determined from the condition

$$\omega_k(H_0, k_s, \phi_k = 0) = \omega_0. \tag{20}$$

Fig. 8(b) displays the dependencies of k_s multiplied by D_0 on the resonance frequency $f_0 = \omega_0/2\pi$. The dependencies were obtained by numerical solution of equation (20) for grain sizes $D_0 = 12$ and 24 nm. This figure also shows the corresponding dependencies $k_{ripple}(f_0)$. For the calculation of $k_{ripple}(f_0) = 1/R_{||}(f_0)$, we used the values of the longitudinal correlation radius $R_{||}$ obtained from the micromagnetic simulation (see Fig. 3b). From Fig. 8 (b), it is easy to understand why there is no sharp broadening of FMR line for the film with $D_0 = 12$ nm. The dependence $k_{ripple}(f_0)$ does not cross the $k_s(f_0)$ curve, therefore, the condition $k_s = k_{ripple}$ cannot be satisfied in the whole frequency range. On the other hand, for the film with $D_0 = 24$ nm the curves $k_{ripple}(f_0)$ and $k_s(f_0)$ intersect at a point $f_0 = f_1$, where the maximum scattering of spin waves on magnetization ripple is observed.

The dependence $f_1(D_0)$ obtained from the condition $k_s = k_{ripple}$ for the films with various grain sizes is shown by triangles in Fig. 7. This dependence correlates well with the micromagnetic simulation results, although the $f_1(D_0)$ values are slightly higher for all points except $D_0 = 100$ nm. The origin of this discrepancy lies in the fact that we calculated $k_s(f_0)$ using the dispersion relation (18) that is valid for homogeneous thin films. In the case of an inhomogeneous magnetic medium, the spin-wave dispersion relation is modified [70,71]. This, in particular, results in the characteristic kinks in the dispersion curves that were observed experimentally [72]. However, this modified relation has a much more complicated form, so we have decided to use a simpler dispersion relation (18) instead.

From this simple theoretical model, we can readily obtain an expression for the critical grain size D_{cr}, above which the effect of sharp FMR line broadening occurs. Fig. 8(b) indicates that k_s increase monotonically with f_0 until a certain limiting value $k_s(\infty)$. Considering (19) and (20) we have

$$k_s(\infty) = \sqrt{2\pi(1 - N_k(k_s, d))}/L_{ex}, \tag{21}$$

where the exchange length $L_{ex} = \sqrt{2A/M_s^2}$ is determined by the competition between the exchange energy and dipolar energy [19].

The monotonically increasing dependencies $k_{ripple}(f_0)$ also tend to a finite value at large f_0. As it was shown in section 3.1, the longitudinal correlation radius $R_{||}$ tends to $R = D_0/2$ at $H \to \infty$, hence $k_{ripple}(\infty) = 2/D_0$. As can be seen from Fig. 8(b), the condition $k_s = k_{ripple}$ can be satisfied only when $k_{ripple}(\infty) \leq k_s(\infty)$. Thus, using the equality $k_{ripple}(\infty) = k_s(\infty)$, we can write the expression for the determination of critical grain size as

$$D_{cr} = g(d/D_{cr}) \cdot L_{ex}. \tag{22}$$

The function $g(d/D_{cr}) = \sqrt{2/\pi(1 - N_k(k = 2/D_{cr}, d))}$ in (22) depends

Table 3
Values of the $g(d/D_{cr})$ function from Eq. (22) for several values of the argument.

d/D_{cr}	0.25	0.5	1	2	3	5	10	100
$g(d/D_{cr})$	1.73	1.32	1.06	0.92	0.87	0.84	0.82	0.80

only on the ratio of grain size to film thickness. Table 3 shows values of the $g(z)$ function for several values of its argument $z = d/D_{cr}$. With the increase of z, the $g(z)$ function rapidly decreases and tends to the constant value of about 0.8. Therefore, for sufficiently thick films (compared to the grain size), the critical size approximately equals $D_{cr} \approx 0.8 \, L_{ex}$. In the case of a monolayer, as it follows from Table 3, the critical size is $D_{cr} \approx L_{ex}$. Calculation of D_{cr} according to expression (22) for the parameters used in the micromagnetic simulation gives a value of 15.7 nm, in accordance with the simulation results shown in Fig. 5.

We should also discuss the approximations used by Arias and Mills to derive expression (16). This expression describes the frequency dependence of the FMR line broadening, and it is widely used in practice. However, expression (16) cannot explain the sharp, resonance-like FMR line broadening revealed with the micromagnetic simulations. Expression (16) was obtained in the limit of an ultrathin film ($kd \ll 1$) having small defects (grains), $kD_0 \ll 1$. The first approximation was used by Arias and Mills to approximate the demagnetization factor (19) by the expression $N_k \approx 1 - kd/2$. This approximation is valid if the quadratic term in an expansion of $M_s N_k$ is much smaller than the quadratic term Dk^2 in (18), that is, the film thickness must be much smaller than the exchange length, $d \ll L_{ex}$. Considering the approximation $kD_0 \ll 1$, the size of defects (grains) also must be substantially smaller than L_{ex}. In other words, the theoretical model of Arias and Mills is valid for a case when $D_0 < D_{cr}$, which is confirmed by the micromagnetic simulation results presented in Fig. 5.

It is interesting to note that such resonance-like behavior of the FMR linewidth frequency dependence has been recently reported for the nanocrystalline thin ferromagnetic films of $Co_{40}Fe_{40}B_{20}$ [73]. In the paper, the authors studied the effect of annealing temperature on the crystallization processes and ferromagnetic resonance parameters of the thin film. They found that with the increase of the annealing temperature the crystallites became larger. But most importantly for us, it was also found that when the crystallite size exceeded a value of about 14 nm, a peak appeared on the linewidth frequency dependence at the frequency of $f_1 \sim 5.5$ GHz, while the resonance field markedly shifted. Moreover, this shift changed sign near f_1. The estimate of f_1 frequency according to expression (17) for the parameters of the $Co_{40}Fe_{40}B_{20}$ film from Ref. [73] gives a value of about 5.3 GHz that is close to the experimental data. The calculation of the critical grain size for the same $Co_{40}Fe_{40}B_{20}$ film parameters according to expression (22) results in $D_{cr} \sim 13.2$ nm, also in accordance with the experiment. Thus, the findings presented in Ref. [73] are possible experimental evidence of the revealed here with the micromagnetic simulation effect of magnetization ripple on the relaxation processes in nanocrystalline thin films.

4. Conclusion

In this work, we investigated the magnetic microstructure and high-frequency susceptibility of nanocrystalline thin films. Using micromagnetic simulation, we calculated correlation characteristics of the inhomogeneous stochastic magnetic structure—magnetization ripple, and its influence on the ferromagnetic resonance. We showed that for the films having the grain size and thickness smaller than a certain critical value, the frequency dependence of the FMR line broadening exhibits the monotonous arcsin-like behavior and can be fairly accurately reproduced by the theoretical predictions of Arias and Mills [63]. However, when the grains become larger and exceed the critical size, the FMR line broadening exhibits a sharp peak at a specific frequency f_1, which depends on the thickness, grain size, and magnetic parameters of the film. This behavior is also accompanied by the substantial shift of the resonance field, with the shift value changing sign near the frequency position of the peak. We demonstrated that the revealed peak of FMR line broadening and resonance field shift are caused by the scattering of spin waves on inhomogeneities of the stochastic magnetic structure and that these effects can be described in the framework of the dynamic magnetization ripple theory developed by Ignatchenko and Degtyarev

[67]. Using a simple two-magnon model of FMR damping in a nanocrystalline thin film, we explained the revealed effect of the sharp FMR line broadening, and we obtained the expression for the determination of the critical grain size D_{cr}. The obtained theoretical results are in good accordance with the experimental data reported by other authors.

CRediT authorship contribution statement

A.V. Izotov: Conceptualization, Methodology, Software, Writing - original draft, Writing – review & editing, Supervision. **B.A. Belyaev:** Conceptualization, Supervision, Writing – review & editing, Funding acquisition. **P.N. Solovev:** Conceptualization, Methodology, Software, Writing - original draft, Writing – review & editing. **N.M. Boev:** Software, Visualization, Writing – review & editing.

Declaration of Competing Interest

The authors declare that they have no known competing financial interests or personal relationships that could have appeared to influence the work reported in this paper.

Acknowledgement

References

[1] J. Petzold, Advantages of softmagnetic nanocrystalline materials for modern electronic applications, J. Magn. Magn. Mater. 242–245 (2002) 84–89, https://doi.org/10.1016/S0304-8853(01)01206-9.

[2] M. Yamaguchi, K. Hyeon Kim, S. Ikedaa, Soft magnetic materials application in the RF range, J. Magn. Magn. Mater. 304 (2006) 208–213, https://doi.org/10.1016/j.jmmm.2006.02.143.

[3] Y. Yoshizawa, S. Oguma, K. Yamauchi, New Fe-based soft magnetic alloys composed of ultrafine grain structure, J. Appl. Phys. 64 (1988) 6044–6046, https://doi.org/10.1063/1.342149.

[4] M. Ohta, Y. Yoshizawa, Effect of heating rate on soft magnetic properties in nanocrystalline Fe80.5Cu1.5Si4B14 and Fe82Cu1Nb1Si4B12 alloys, Appl. Phys Express 2 (2009), 023005, https://doi.org/10.1143/APEX.2.023005.

[5] H. Lee, K.-J. Lee, Y.-K. Kim, K. Kim, S.-C. Yu, Ultra-soft magnetic properties in nanocrystalline Fe81B11Nb7Cu1 alloy, J. Alloy. Compd. 326 (2001) 313–316, https://doi.org/10.1016/S0925-8388(01)01291-9.

[6] K. Suzuki, N. Kataoka, A. Inoue, A. Makino, T. Masumoto, High saturation magnetization and soft magnetic properties of bcc Fe-Zr-B alloys with ultrafine grain structure, Mater. Trans., JIM 31 (1990) 743–746, https://doi.org/10.2320/matertrans1989.31.743.

[7] G. Herzer, Modern soft magnets: Amorphous and nanocrystalline materials, Acta Mater. 61 (2013) 718–734, https://doi.org/10.1016/j.actamat.2012.10.040.

[8] M.A. Willard, D.E. Laughlin, M.E. McHenry, D. Thoma, K. Sickafus, J.O. Cross, V. G. Harris, Structure and magnetic properties of (Fe0.5Co0.5)88Zr7B4Cu1 nanocrystalline alloys, J. Appl. Phys. 84 (1998) 6773–6777, https://doi.org/10.1063/1.369007.

[9] Y. Suzuki, S. Fujii, D.H. Ping, M. Ohnuma, K. Hono, Magnetic properties of nanocrystalline FeMCuNbSiB alloys (M: Co, Ni), Scr. Mater. 48 (2003) 863–868, https://doi.org/10.1016/S1359-6462(02)00611-5.

[10] I. Fergen, K. Seemann, A.v.d. Weth, A. Schüppen, Soft ferromagnetic thin films for high frequency applications, J. Magn. Magn. Mater. 242–245 (2002) 146–151, https://doi.org/10.1016/S0304-8853(01)01185-4.

[11] S.M. Choi, T. Lee, C.-S. Yang, K.-H. Shin, S.H. Lim, Effects of lateral dimensions of the magnetic thin films on the characteristics of thin-film type orthogonal fluxgate sensors, Thin Solid Films 565 (2014) 271–276, https://doi.org/10.1016/j.tsf.2014.06.026.

[12] J. Deak, A. Jander, E. Lange, S. Mundon, D. Brownell, L. Tran, Delta-sigma digital magnetometer utilizing bistable spin-dependent-tunneling magnetic sensors, J. Appl. Phys. 99 (2006) 08B320, https://doi.org/10.1063/1.2171942.

[13] T. Morikawa, Y. Nishibe, H. Yamadera, Y. Nonomura, M. Takeuchi, J. Sakata, Y. Taga, Enhancement of giant magneto-impedance in layered film by insulator separation, IEEE Trans. Magn. 32 (1996) 4965–4967, https://doi.org/10.1109/20.539303.

[14] A.N. Babitskii, B.A. Belyaev, N.M. Boev, G.V. Skomorokhov, A.V. Izotov, R. G. Galeev, A magnetometer of weak quasi-stationary and high-frequency fields on resonator microstrip transducers with thin magnetic fields, Instrum. Exp. Tech. 59 (2016) 425–432, https://doi.org/10.1134/S0020441216030131.

[15] H. Uetake, T. Kawakami, S. Yabukami, T. Ozawa, N. Kobayashi, K.I. Arai, Highly sensitive coplanar line thin-film sensor using SrTiO film, IEEE Trans. Magn. 50 (2014) 1–4, https://doi.org/10.1109/TMAG.2014.2331676.

[16] C.V. Falub, R. Hida, M. Meduna, J. Zweck, J.-P. Michel, H. Sibuet, D. Schneider, M. Bless, J.H. Richter, H. Rohrmann, Structural and ferromagnetic properties of sputtered FeCoB/AlN soft magnetic multilayers for GHz applications, IEEE Trans. Magn. 53 (2017) 1–6, https://doi.org/10.1109/TMAG.2017.2703175.

[17] A.N. Lagarkov, K.N. Rozanov, High-frequency behavior of magnetic composites, J. Magn. Magn. Mater. 321 (2009) 2082–2092, https://doi.org/10.1016/j.jmmm.2008.08.099.

[18] O. Acher, A.L. Adenot, Bounds on the dynamic properties of magnetic materials, Phys. Rev. B. 62 (2000) 11324–11327, https://doi.org/10.1103/PhysRevB.62.11324.

[19] S. Shukla, P.K. Deheri, R.V. Ramanujan, Magnetic Nanostructures: Synthesis, Properties, and Applications, in: R. Vajtai (Ed.), Springer Handbook of Nanomaterials, Springer, Berlin Heidelberg, Berlin, Heidelberg, 2013, pp. 473–514, https://doi.org/10.1007/978-3-642-20595-8_12.

[20] T.J. Klemmer, K.A. Ellis, L.H. Chen, B. van Dover, S. Jin, Ultrahigh frequency permeability of sputtered Fe–Co–B thin films, J. Appl. Phys. 87 (2000) 830–833, https://doi.org/10.1063/1.371949.

[21] A.R. Chezan, C.B. Craus, N.G. Chechenin, L. Niesen, D.O. Boerma, Structure and soft magnetic properties of Fe-Zr-N films, Phys. Stat. Sol. (a) 189 (2002) 833–836, https://doi.org/10.1002/1521-396X(200202)189:3<833::AID-PSSA833>3.0.CO;2-B.

[22] J. Lou, R.E. Insignares, Z. Cai, K.S. Ziemer, M. Liu, N.X. Sun, Soft magnetism, magnetostriction, and microwave properties of FeGaB thin films, Appl. Phys. Lett. 91 (2007), 182504, https://doi.org/10.1063/1.2804123.

[23] D. Cronin, D. Lordan, G. Wei, P. McCloskey, C.O. Mathúna, A. Masood, Soft magnetic nanocomposite CoZrTaB–SiO2 thin films for high-frequency applications, Applied Physics. 127 (2020), 243903, https://doi.org/10.1063/5.0013416.

[24] N. Kataoka, T. Shima, H. Fujimori, High frequency permeability of nanocrystalline Fe–Cu–Nb–Si–B single and multilayer films, J. Appl. Phys. 70 (1991) 6238, https://doi.org/10.1063/1.350007.

[25] H. Greve, C. Pochstein, H. Takele, V. Zaporojtchenko, F. Faupel, A. Gerber, M. Frommberger, E. Quandt, Nanostructured magnetic Fe–Ni–Co/Teflon multilayers for high-frequency applications in the gigahertz range, Appl. Phys. Lett. 89 (2006), 242501, https://doi.org/10.1063/1.2402877.

[26] K. Ikeda, K. Kobayashi, M. Fujimoto, Multilayer nanogranular magnetic thin films for GHz applications, J. Appl. Phys. 92 (2002) 5395–5400, https://doi.org/10.1063/1.1510562.

[27] G. Herzer, Nanocrystalline soft magnetic materials, J. Magn. Magn. Mater. 157 (158) (1996) 133–136, https://doi.org/10.1016/0304-8853(95)01126-9.

[28] R. Alben, J.J. Becker, M.C. Chi, Random anisotropy in amorphous ferromagnets, J. Appl. Phys. 49 (1978) 1653–1658, https://doi.org/10.1063/1.324881.

[29] G. Herzer, Grain size dependence of coercivity and permeability in nanocrystalline ferromagnets, IEEE Trans. Magn. 26 (1990) 1397–1402, https://doi.org/10.1109/20.104389.

[30] K. Suzuki, G. Herzer, Soft Magnetic Nanostructures and Applications, in: D. Sellmyer, R. Skomski (Eds.), Advanced Magnetic Nanostructures, Kluwer Academic Publishers, Boston, 2006: pp. 365–401. 10.1007/0-387-23316-4_13.

[31] S. Thomas, S.H. Al-Harthi, D. Sakthikumar, I.A. Al-Omari, R.V. Ramanujan, Y. Yoshida, M.R. Anantharaman, Microstructure and random magnetic anisotropy in Fe-Ni based nanocrystalline thin films, Appl. Phys. 41 (2008), 155009, https://doi.org/10.1088/0022-3727/41/15/155009.

[32] T. Hysen, S. Al-Harthi, I.A. Al-Omari, P. Geetha, R. Lisha, R.V. Ramanujan, D. Sakthikumar, M.R. Anantharaman, Annealing induced low coercivity, nanocrystalline Co–Fe–Si thin films exhibiting inverse cosine angular variation, J. Magn. Magn. Mater. 341 (2013) 165–172, https://doi.org/10.1016/j.jmmm.2013.04.032.

[33] R. Fersi, Study of exchange interaction, magnetization correlations and random magnetic anisotropy in nanocrystalline Pr2Co7 films deposited on Si substrate, J. Magn. Magn. Mater. 494 (2020), 165816, https://doi.org/10.1016/j.jmmm.2019.165816.

[34] H. Hoffmann, Theory of magnetization ripple, IEEE Trans. Magn. 4 (1968) 32–38, https://doi.org/10.1109/TMAG.1968.1066186.

[35] H. Hoffmann, Quantitative calculation of the magnetic ripple of uniaxial thin permalloy films, J. Appl. Phys. 35 (1964) 1790–1798, https://doi.org/10.1063/1.1713743.

[36] T. Suzuki, Investigations into ripple wavelength in evaporated thin films by lorentz microscopy, phys. Stat. Sol. (b) 37 (1970) 101–114, https://doi.org/10.1002/pssb.19700370113.

[37] K.J. Harte, Theory of magnetization ripple in ferromagnetic films, J. Appl. Phys. 39 (1968) 1503–1524, https://doi.org/10.1063/1.1656388.

[38] V.A. Ignatchenko, Magnetic structure of thin magnetic films and ferromagnetic resonance, Soviet Physics JETP. 27 (1) (1968) 162–166.

[39] H. Kronmuller, S. Parkin, Handbook of Magnetism and Advanced Magnetic Materials, John Wiley & Sons, Chichester, 2007.

[40] D.V. Berkov, N.L. Gorn, Numerical simulation of the magnetization structures in thin polycrystalline films with the random anisotropy and intergrain exchange, J. Appl. Phys. 83 (1998) 6350–6352, https://doi.org/10.1063/1.367913.

[41] B.A. Belyaev, A.V. Izotov, P.N. Solovev, Numerical simulation of magnetic microstructure in nanocrystalline thin films with the random anisotropy, J. Siberian Federal Univ. Math. Phys. 10 (2017) 132–135. 10.17516/1997-1397-2017-10-1-132-135.

[42] S.V. Komogortsev, V.A. Fel'k, R.S. Iskhakov, G.V. Shadrina, Micromagnetism in a planar system with a random magnetic anisotropy and two-dimensional magnetic

correlations, J. Exp. Theor. Phys. 125 (2017) 323–332, https://doi.org/10.1134/S1063776117070196.

[43] A. Bachleitner-Hofmann, B. Bergmair, T. Schrefl, A. Satz, D. Suess, Soft magnetic properties of thin nanocrystalline particles due to the interplay of random and coherent anisotropies, IEEE Trans. Magn. 53 (2017) 1–6, https://doi.org/10.1109/TMAG.2017.2695580.

[44] B.A. Belyaev, A.V. Izotov, An.A. Leksikov, Micromagnetic calculation of the equilibrium distribution of magnetic moments in thin films, Phys. Solid State 52 (2010) 1664–1672, https://doi.org/10.1134/S1063783410080160.

[45] P.N. Solovev, A.V. Izotov, B.A. Belyaev, Microstructural and magnetic properties of thin obliquely deposited films: a simulation approach, J. Magn. Magn. Mater. 429 (2017) 45–51, https://doi.org/10.1016/j.jmmm.2017.01.012.

[46] P.N. Solovev, A.V. Izotov, B.A. Belyaev, Micromagnetic simulation of magnetization reversal processes in thin obliquely deposited films, J. Siberian Federal Univ. Math. Phys. 9 (2016) 524–527. 10.17516/1997-1397-2016-9-4-524-527.

[47] B.A. Belyaev, N.M. Boev, A.V. Izotov, P.N. Solovev, Study of peculiarities of the microwave absorption spectrum of nanocrystalline thin magnetic films, Russ. Phys. J. 61 (2019) 1798–1805, https://doi.org/10.1007/s11182-019-01603-4.

[48] R.D. McMichael, D.J. Twisselmann, A. Kunz, Localized ferromagnetic resonance in inhomogeneous thin films, Phys. Rev. Lett. 90 (2003), 227601, https://doi.org/10.1103/PhysRevLett.90.227601.

[49] A.V. Izotov, B.A. Belyaev, P.N. Solovev, N.M. Boev, Numerical calculation of high frequency magnetic susceptibility in thin nanocrystalline magnetic films, Physica B 556 (2019) 42–47, https://doi.org/10.1016/j.physb.2018.12.006.

[50] M.A. Willard, M. Daniil, Nanocrystalline soft magnetic alloys two decades of progress, Handbook of Magnetic Materials, Elsevier (2013) 173–342, https://doi.org/10.1016/B978-0-444-59593-5.00004-0.

[51] A. Michels, S. Erokhin, D. Berkov, N. Gorn, Micromagnetic simulation of magnetic small-angle neutron scattering from two-phase nanocomposites, J. Magn. Magn. Mater. 350 (2014) 55–68, https://doi.org/10.1016/j.jmmm.2013.09.031.

[52] J. Leliaert, A. Vansteenkiste, A. Coene, L. Dupré, B. Van Waeyenberge, Vinamax: a macrospin simulation tool for magnetic nanoparticles, Med. Biol. Eng. Compu. 53 (2015) 309–317, https://doi.org/10.1007/s11517-014-1239-6.

[53] S.-J. Lee, S. Sato, H. Yanagihara, E. Kita, C. Mitsumata, Numerical simulation of random magnetic anisotropy with solid magnetization grains, J. Magn. Magn. Mater. 323 (2011) 28–31, https://doi.org/10.1016/j.jmmm.2010.08.015.

[54] A.J. Newell, W. Williams, D.J. Dunlop, A generalization of the demagnetizing tensor for nonuniform magnetization, J. Geophys. Res. 98 (1993) 9551, https://doi.org/10.1029/93JB00694.

[55] K.M. Lebecki, M.J. Donahue, M.W. Gutowski, Periodic boundary conditions for demagnetization interactions in micromagnetic simulations, J. Phys. D Appl. Phys. 41 (2008), 175005, https://doi.org/10.1088/0022-3727/41/17/175005.

[56] B.A. Belyaev, A.V. Izotov, G.V. Skomorokhov, P.N. Solovev, Experimental study of the magnetic characteristics of nanocrystalline thin films: the role of edge effects, Mater. Res. Express 6 (2019) 116105, https://doi.org/10.1088/2053-1591/ab4456.

[57] Z. Hussain, D. Kumar, V.R. Reddy, A. Gupta, Kerr microscopy study of exchange-coupled FePt/Fe exchange spring magnets, J. Magn. Magn. Mater. 430 (2017) 78–84, https://doi.org/10.1016/j.jmmm.2017.01.052.

[58] R.S. Iskhakov, V.A. Ignatchenko, S.V. Komogortsev, A.D. Balaev, Study of magnetic correlations in nanostructured ferromagnets by correlation magnetometry, JETP Lett. 78 (2003) 646–650, https://doi.org/10.1134/1.1644310.

[59] A. Michels, R.N. Viswanath, J.G. Barker, R. Birringer, J. Weissmüller, Range of magnetic correlations in nanocrystalline soft magnets, Phys. Rev. Lett. 91 (2003), 267204, https://doi.org/10.1103/PhysRevLett.91.267204.

[60] A.G. Gurevich, G.A. Melkov, Magnetization Oscillations and Waves, CRC Press, Boca Raton, 1996.

[61] R.D. McMichael, P. Krivosik, Classical model of extrinsic ferromagnetic resonance linewidth in ultrathin films, IEEE Trans. Magn. 40 (2004) 2–11, https://doi.org/10.1109/TMAG.2003.821564.

[62] S.S. Kalarickal, P. Krivosik, J. Das, K.S. Kim, C.E. Patton, Microwave damping in polycrystalline Fe-Ti-N films: physical mechanisms and correlations with composition and structure, Phys. Rev. B 77 (2008), 054427, https://doi.org/10.1103/PhysRevB.77.054427.

[63] R. Arias, D.L. Mills, Extrinsic contributions to the ferromagnetic resonance response of ultrathin films, Phys. Rev. B 60 (1999) 7395–7409, https://doi.org/10.1103/PhysRevB.60.7395.

[64] I. Barsukov, F.M. Römer, R. Meckenstock, K. Lenz, J. Lindner, S. Hemken to Krax, A. Banholzer, M. Körner, J. Grebing, J. Fassbender, M. Farle, Frequency dependence of spin relaxation in periodic systems, Phys. Rev. B 84 (2011) 140410 (R). 10.1103/PhysRevB.84.140410.

[65] H. Kurebayashi, T.D. Skinner, K. Khazen, K. Olejník, D. Fang, C. Ciccarelli, R. P. Campion, B.L. Gallagher, L. Fleet, A. Hirohata, A.J. Ferguson, Uniaxial anisotropy of two-magnon scattering in an ultrathin epitaxial Fe layer on GaAs, Appl. Phys. Lett. 102 (2013), 062415, https://doi.org/10.1063/1.4792269.

[66] J. Lindner, I. Barsukov, C. Raeder, C. Hassel, O. Posth, R. Meckenstock, P. Landeros, D.L. Mills, Two-magnon damping in thin films in case of canted magnetization: theory versus experiment, Phys. Rev. B 80 (2009), 224421, https://doi.org/10.1103/PhysRevB.80.224421.

[67] V.A. Ignatchenko, G.V. Degtyarev, Resonant Shift and Broadening of FMR Lines, Due to Fine Magnetic Structure, Soviet Physics JETP 33 (2) (1971) 393–397.

[68] P. Landeros, D.L. Mills, Spin waves in periodically perturbed films, Phys. Rev. B 85 (2012), 054424, https://doi.org/10.1103/PhysRevB.85.054424.

[69] M. Körner, K. Lenz, R.A. Gallardo, M. Fritzsche, A. Mücklich, S. Facsko, J. Lindner, P. Landeros, J. Fassbender, Two-magnon scattering in permalloy thin films due to rippled substrates, Phys. Rev. B 88 (2013), 054405, https://doi.org/10.1103/PhysRevB.88.054405.

[70] V.A. Lgnatchenko, R.S. Iskhakov, Spin waves in a randomly inhomogeneous anisotropic medium, Sov. Phys. JETP. 45 (1977) 526–532.

[71] V.A. Lgnatchenko, R.S. Lskhakov, Spin waves in amorphous and finely divided ferromagnets with allowance for dipole-dipole interaction, Sov. Phys. JETP. 47 (1978) 725–729.

[72] V.A. Ignatchenko, R.S. Iskhakov, L.A. Chekanova, N.S. Chistyakov, Study of the dispersion law for spin waves in amorphous films by the spin-wave resonance method, Sov. Phys. JETP. 48 (1978) 328–330.

[73] R.A. O'Dell, A.B. Phillips, D.G. Georgiev, J.G. Jones, G.J. Brown, M.J. Heben, Post-deposition annealing effects on ferromagnetic CoFeB thin films, IEEE Trans. Magn. 54 (2018) 1–7, https://doi.org/10.1109/TMAG.2018.2845394.